Theoretical modeling of XBn T2SLs InAs/InAsSb/B-AlAsSb mid-wave detector operating below thermoelectrical cooling

P. Martyniuk[1], K. Michalczewski[1], T. Y. Tsai[2], C. H. Wu[2], Y. R. Wu[2]

[1] Institute of Applied Physics, Military University of Technology, 2 Urbanowicza Str., 00-908 Warsaw, Poland
(✉piotr.martyniuk@wat.edu.pl, +48 261839215)
[2] Graduate Institute of Photonics and Optoelectronics, National Taiwan University, Roosevelt Str., 10617 Taipei, Taiwan

***Abstract*–The paper reports on the barrier mid-wave infrared InAs/InAsSb (x_{Sb} = 0.4) type-II superlattice operating below thermoelectrical cooling. AlAsSb (x_{Sb} = 0.97) barrier was proved to be proper material not introducing extra barrier in valence band in analyzed temperature range. The highest detectivity of the simulated structure was assessed at the level of ~ 10^{12} Jones at T ~ 100 K.**

I. INTRODUCTION

Infrared detectors have many applications in civilian and military environment. Currently, many of these infrared applications requires high-performance Mercury Cadmium Telluride (MCT) photodetectors. Due to higher cost of the MCT, antimonide based type-II superlattices (T2SLs) have been proposed as an alternative with lower fabrication cost and better performance with low dark current due to suppressed Auger generation-recombination (GR) rate and tunneling current [1,2]. It must be underlined that those theoretical predictions has not been reached yet. The limiting factor of the widely studied T2SLs InAs/GaSb is the short minority carrier lifetime. That could be circumvented by "Ga-free" T2SLs InAs/InAsSb revealing very encouraging results in terms of carrier lifetime ~ 400 ns due to strong suppression of nonradiative recombination [3–5]. Expect material, it has been demonstrated that the XBn structure suppresses the dark current in infrared photodetectors effectively through bandgap engineering [6]. In this paper, we demonstrate theoretical modeling of MWIR XBn photodetectors with T2SLs InAs/InAsSb active layer where AlAsSb barrier was incorporated. It is shown that AlAsSb (x_{Sb} = 0.97) does not introduce extra barriers in valence band of the XBn structure.

II. SIMULATION PROCEDURE AND RESULTS

The nominal simulated T2SLs InAs/InAsSb/B-AlAsSb barrier structure is presented in Fig. 1.

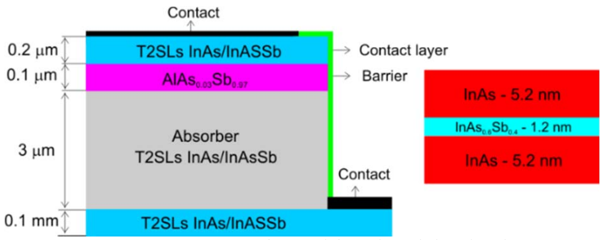

Fig. 1. MWIR T2SLs InAs/InAsSb/B-AlAsSb barrier detector.

The T2SLs InAs/InAsSb contact layers (0.2 µm n/p-type, 10^{16} cm^{-3} and 0.1 µm n-type 5×10^{17} cm^{-3}) and absorber (3 µm, 5×10^{15} cm^{-3}) were assumed to have 5.2 nm (InAs) and 1.2 nm (InAsSb) while Sb composition x_{Sb} = 0.4. The 0.1 nm, n-type 10^{16} cm^{-3} AlAsSb (x_{Sb} = 0.97) barrier was introduced to the detector's structure.

Table 1. Material parameters taken in modeling of T2SLs InAs/InAsSb.

Parameters	**Symbols**	**GaAs**	**InAs**	**InSb**	**GaSb**
Lattice constant a(T)=a(T=300K)+a_T×(T-300)	a_T(Å/K)	3.88×10^{-5}	2.74×10^{-5}	3.48×10^{-5}	4.72×10^{-5}
	a(T=300K)(Å)	5.65325	6.0583	6.4794	6.0959
Bandgap E_g^Γ(T)= E_g^Γ(T=0K) - $\frac{\alpha T^2}{T+\beta}$	α(meV/K)	0.5405	0.276	0.32	0.417
	β(K)	204	93	170	140
	E_g^Γ(T=0K) (eV)	1.519	0.417	0.25	0.812
Luttinger parameters	γ_1	7.05	20.0	34.8	13.4
	γ_2	2.35	8.5	15.5	4.7
	γ_3	3	9.2	16.5	6
Deformation potentials	a_c(eV)	-7.17	-5.08	-6.94	-7.5
	$a_v(eV)$	-1.16	-1	-0.36	-0.8
	b(eV)	-2	-1.8	-2	-2
	d(eV)	-4.8	-3.6	-4.7	-4.7
Elastic constant	C_{11}(GPa)	1221	832.9	684.7	884.2
	C_{12}(GPa)	566	452.6	373.5	402.6
	C_{44}(GPa)	600	395.9	311.1	432.2
Spin-orbit energy	Δ_0(eV)	0.341	0.39	0.82	0.76
Kane potential	E_p(eV)	23.81	21.5	24.08	24.76
Electron affinity	(eV)	4.07	4.9	4.59	4.06
Valence band offset	VBO(eV)	-0.8	-0.59	0	-0.03
Effective mass (0K)	$\frac{m_e^*}{m_0}$	0.064	0.023	0.0138	0.038

Table 2. Bowing parameters for InAsSb.

Bowing parameters	E_g^Γ(eV)	0.67
	Δ_0(eV)	1.2
	$m_e^*(\Gamma)$	0.035

The 8×8 kp method was used to calculate bandgap energy and effective masses in plane and growth direction for T2SLs InAs/InAsSb. The material parameters assumed in T2SLs InAs/InAsSb modeling are presented in Table 1 and 2 [7]. The T2SLs InAs/InAsSb bandgap energy versus temperature and fitted Varshni equation are presented in Fig. 2 (a) while electron and hole effective masses are presented in Fig. 2 (b). Detector structure was simulated with software APSYS by Crosslight Inc. using bulk based model.

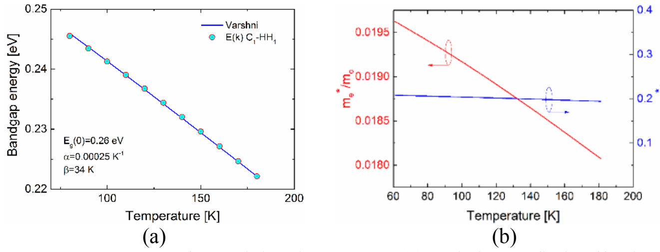

(a) (b)

Fig. 2. T2SLs InAs/InAsSb bandgap energy (a) and electron/hole effective masses (b) versus temperature.

Calculated energy band diagrams for nB_nnn^+ and pB_nnn^+ were presented in Fig. 3 (a) and (b) respectively for 80 K and unbiased condition. For n-type contact layer extra barrier in valence band is visible while barrier in conduction band is close to 1.5 eV.

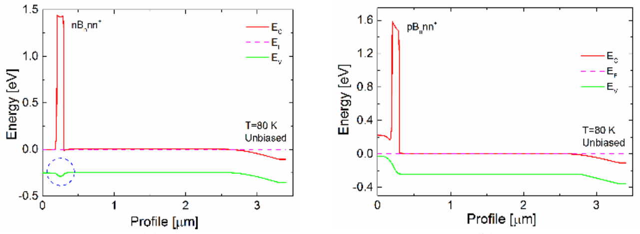

(a) (b)

Fig. 3. Energy band diagram for MWIR T2SLs InAs/InAsSb/B-AlAsSb barrier structure for two detector's architectures: nB$_n$nn$^+$ (a) and pB$_n$nn$^+$ (b) for unbiased condition simulated for $T = 80$ K.

Dark current characteristics versus reciprocal temperature for two detector's architectures: nB$_n$nn$^+$ and pB$_n$nn$^+$ are presented in Fig. 4 (a) and (b).

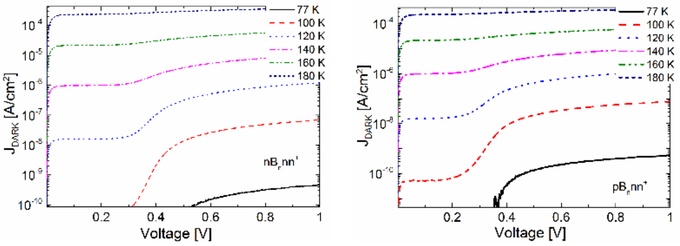

(a) (b)

Fig. 4. Dark current for detector's architectures: nB$_n$nn$^+$ (a) and pB$_n$nn$^+$ (b) versus voltage for selected temperatures: 77–180 K.

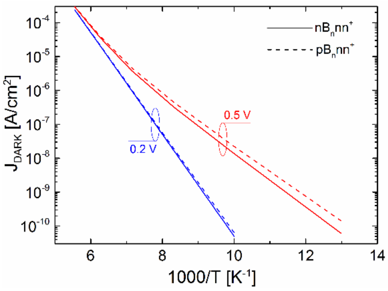

Fig. 5. Dark current for two detector's architectures: nB$_n$nn$^+$/pB$_n$nn$^+$ versus reciprocal temperature and selected voltages: 0.2 V and 0.5 V.

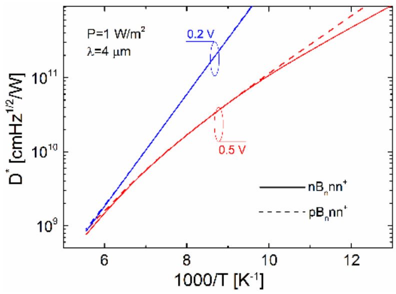

Fig. 6. Detectivity for two detector's architectures: nB$_n$nn$^+$/pB$_n$nn$^+$ versus reciprocal temperature and selected voltages: 0.2 V and 0.5 V.

Detectivity was calculated assuming thermal Johnson-Nyquist and shot noises according to the relation:

$$D^* = \frac{R_i}{\left(\frac{4k_BT}{RA}+2qJ_{DARK}\right)^{0.5}} \qquad (1)$$

where: R_i, k_B, R, A, stands for current responsivity, Boltzmann constant, resistance and detector's electrical area.

III. CONCLUSIONS

We demonstrated theoretical modeling of MWIR XBn photodetectors with T2SLs InAs/InAsSb active layer where AlAsSb barrier was implemented. It was shown that material does not introduce extra barriers in valence band in analyzed XBn structure. The highest detectivity of the simulated structure was assessed at the level of ~ 10^{12} Jones for $T \sim 100$ K.

ACKNOWLEDGMENT

This paper has been completed with the financial support of The National Centre for Research and Development-the grant no. PL-TW4/3/2017.

REFERENCES

[1] D. Z.-Y. Ting, A. Soibel, L. Höglund, J. Nguyen, C.J. Hill, A. Khoshakhlagh, and S.D. Gunapala, "Type-II superlattice infrared detectors", in *Semiconductors and Semimetals*, vol. 84, pp. 1–57, edited by S.D. Gunapala, D.R. Rhiger, and C. Jagadish, Elsevier, Amsterdam, 2011.

[2] D. Lackner, M. Steger, M. L. W. Thewalt, O. J. Pitts, Y. T. Cherng et al. "InAs/InAsSb strain balanced superlattices for optical detectors: Material properties and energy band simulations", J. Appl. Phys. 111, 034507 (2012).

[3] T. Schuler-Sandy, S. Myers, B. Klein, N. Gautam, P. Ahirwar, Z.-B. Tian, T. Rotter, G. Balakrishnan, E. Plis, and S. Krishna, "Gallium free type II InAs/InAs$_x$Sb$_{1-x}$ superlattice photodetectors", Appl. Phys. Lett. 101, 071111 (2012).

[4] E. H. Steenbergen, B. C. Connelly, G. D. Metcalfe, H. Shen, M. Wraback, D. Lubyshev, Y. Qiu, J. M. Fastenau, A. W. K. Liu, S. Elhamri, O. O. Cellek, Y.-H. Zhang, "Significantly improved minority carrier lifetime observed in a long-wavelength infrared III-V type-II superlattice comprised of InAs/InAsSb", Appl. Phys. Lett. 99, 251110 (2011).

[5] L. Höglund, D. Z. Ting, A. Khoshakhlagh, A. Soibel, C. J. Hill, A. Fisher, S. Keo, and S. D. Gunapala, "Influence of radiative and non-radiative recombination on the minority carrier lifetime in midwave infrared InAs/InAsSb superlattices", Appl. Phys. Lett. 103, 221908 (2013).

[6] S. Maimon, G. W. Wicks, "nBn detector, an infrared detector with reduced dark current and higher operating temperature", Appl. Phys. Lett. 89, 151109 (2006).

[7] I. Vurgaftman, J. R. Meyer, "Band parameters for III–V compound semiconductors and their alloys", J. Appl. Phys. 89, 5815 (2001).